Available online at www.sciencedirect.com

ScienceDirect

Procedia Structural Integrity 2 (2016) 2462–2254

Structural Integrity Procedia

www.elsevier.com/locate/procedia

21st European Conference on Fracture, ECF21, 20-24 June 2016, Catania, Italy

3D J-integral for functionally graded and temperature dependent thermoelastic materials

J. Hein, M. Kuna*

Institute of Mechanics and Fluid Dynamics, Technical University Freiberg, Lampadiusstraße 4, 09599 Freiberg, Germany

Abstract

In order to mitigate the thermal shock impact, many ceramics, refractories or heat protecting layers are made of functionally graded (FGM) or layered structures. Fracture mechanical methods are needed to evaluate the resistance of such structures against failure under thermal shock. Despite a lot of theoretical work has been done for two-dimensional crack configurations in thermoelastic FGM, real defects and structural components are of three-dimensional (3D) nature. In most cases the real gradation of the thermoelastic material properties does not obey simple mathematical functions, but show a complex dependency on location due to manufacturing. Moreover, the elastic and thermodynamic properties depend on temperature itself. In the paper, we present the derivation of the 3D J-integral for arbitrary location and temperature dependent material behavior. The J-integral is implemented in FEM by means of the equivalent domain integral technique. The method is applied to a thermally loaded plate of FGM with a surface crack. The influence of the material gradation on the results is investigated in various examples.

Keywords: J-integral ; functionally graded material ; temperature dependent material ; 3D crack ; thermal shock

Nomenclature

α	thermal expansion coefficient
δ_{ij}	Kronecker symbol
ϵ_{ij}	strain tensor consisting of mechanical $\epsilon_{ij}^{\mathrm{m}}$ and thermal strain tensor $\epsilon_{ij}^{\mathrm{th}}$
Φ	synonym for a material property
σ_{ij}	stress tensor
ΔA	virtually extended crack area along a crack segment Δs
Δa	crack growth
Δl_m	virtual crack propagation vector
a	crack length

* Corresponding author. Tel.: +49-3731-39-2092 ; fax: +49-373-39-3455
E-mail address: meinhard.kuna@imfd.tu-freiberg.de

10.1016/j.prostr.2016.06.281

C_{ijkl}	elasticity tensor
f_p	amount of pore forming agents in the ceramic
G	energy release rate
J_i	J-vector
$\overline{J}$	released energy (related to virtually extended crack area ΔA)
n_i	normal vector on integration contour
q	smoothly varying weighting function
s	crack front position
T	temperature
t_i	traction vector
U	strain energy density
u_i	displacement vector
v_i	direction vector of crack propagation
$\mathbf{x}$	coordinate vector with components x_i

1. Introduction

Due to their favorable mechanical properties, functionally graded materials (FGM) and structures have gained increasing engineering applications, e. g. in thermal barrier coatings, refractory materials or transition layers between dissimilar materials. Meanwhile, there exist several additive or generative technologies to manufacture graded structures like 3D printing, laser sintering etc. Under service conditions, FGM are often exposed to transient temperature fields by thermal shock loading. One problem, especially with ceramic FGM is their inherent brittleness and the more complicated stress analysis of cracks. Several finite element techniques (FEM) have been developed to calculate stress intensity factors or energy release rate for cracks in FGM in 2D or 3D structures. The solution requires a staggered thermomechanical finite element analysis, whereby the transient temperature field is firstly obtained from a thermal analysis, which is then employed as loading condition in a subsequent thermoelastic stress analysis step. In both cases the spatial gradation and the temperature dependence of material properties have to be taken into account. The following short literature review is restricted to 3D thermomechanical crack analyses in FGM. Walters et al. (2004) used the equivalent domain form of the J-integral to investigate planar 3D cracks under stationary thermomechanical mode I loading. Yildirim et al. (2005) employed a displacement interpretation technique when studying semi-elliptical surface cracks in a coating subjected to transient thermal loading. To investigate non-planar crack shapes subjected to steady state temperature gradients, Moghaddam and Alfano (2015) employed the interaction integral method to differentiate between mode I and mode II K-factors.

In most of the fracture analyses presented in the literature, simple arbitrarily chosen mathematical functions were assumed for the spatial gradation. So, Nami and Eskandari (2012) used exponential functions to vary elastic modulus and thermal expansion coefficient through the thickness of a FGM cylinder under pressure and steady state thermal fields. Here, we use a true physical relationship for porous ceramics, based on the effect of pore forming agents on all relevant mechanical and thermal material properties. As novelty, the severe dependence of thermomechanical material properties of FGM on temperature is taken into account, which is regarded as necessary for thermal shock scenarios.

2. J-integral for location and temperature dependent material

Figure 1 illustrates the domain $A_{\mathrm{C_c}}$, bounded by the closed contour $C_\mathrm{C} = C_\mathrm{gr} + C^+ - C + C^-$. Hein and Kuna (2014) described the energy release rate G for this 2D crack by

$$G = J = \lim_{r\to 0} \int_C \left(U(x_i, \epsilon_{ij}^\mathrm{m}, T) n_1 - t_i u_{i,1} \right) \mathrm{d}s = \lim_{r\to 0} \left(-I_1 - I_2 + I_3\right) \tag{1}$$

with

$$I_1 = \int_{A_{C_c}} \left(\frac{1}{2} \epsilon_{ij}^{m} \frac{\partial C_{ijkl}}{\partial x_1} \epsilon_{kl}^{m} + \frac{1}{2} \epsilon_{ij}^{m} \frac{\partial C_{ijkl}}{\partial T} \epsilon_{kl}^{m} \frac{\partial T}{\partial x_1} - \sigma_{ij} \left(\left(\frac{\partial \alpha}{\partial x_1} + \frac{\partial \alpha}{\partial T} \frac{\partial T}{\partial x_1} \right) \Delta T(x_i) + \alpha(x_i, T(x_i)) \frac{\partial \Delta T(x_i)}{\partial x_1} \right) \delta_{ij} \right) q \, \mathrm{d}A, \quad (2)$$

$$I_2 = \int_{A_{C_c}} \left(U \delta_{1k} - \sigma_{ik} u_{i,1} \right) q_{,k} \, \mathrm{d}A, \quad (3)$$

$$I_3 = \int_{C^+ + C^-} \left(U n_1 - t_i u_{i,1} \right) q \, \mathrm{d}s. \quad (4)$$

Hereby, $\epsilon_{ij}^{m} = \epsilon_{ij} - \epsilon_{ij}^{th}$ is the mechanical strain tensor, C_{ijkl} elasticity tensor, σ_{ij} stress tensor, α thermal expansion coefficient, U the strain energy density, $t_i = \sigma_{ij} n_j$ traction vector and $q = q(\mathbf{x})$ is a function that varies smoothly within A_{C_c}

$$q(\mathbf{x}) = \begin{cases} 0 \text{ on } C_{gr} \\ 1 \text{ on } C \end{cases} . \quad (5)$$

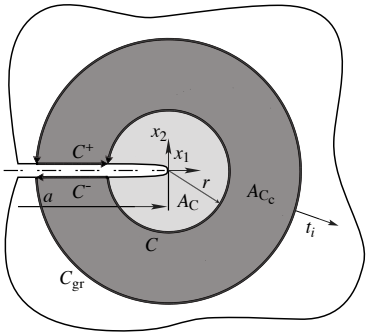

Fig. 1: Integration paths around the crack tip (compare Kuna (2013)).

In case of a crack propagation in x_1-direction the energy release rate is described by $G = J = J_1$. Thereby, J_1 is the first component of the J-vector

$$J_m = \lim_{r \to 0} \int_C \left(U(x_i, \epsilon_{ij}^{m}, T) n_m - t_i u_{i,m} \right) \mathrm{d}s = \lim_{r \to 0} \int_C \left(U n_m - \sigma_{ij} n_j u_{i,m} \right) \mathrm{d}s = \lim_{r \to 0} \int_C \left(U \delta_{mj} - \sigma_{ij} u_{i,m} \right) n_j \mathrm{d}s$$
$$= \lim_{r \to 0} \int_C Q_{mj} n_j \mathrm{d}s \,, \quad m = 1, 2, 3. \quad (6)$$

When dealing with 3D problems, the crack tip becomes a crack front line. If the contour C is moved along the crack front by a small segment Δs, the cylindrical surface S_C is created as sketched in Fig. 2.
Assuming a virtual crack extension $\Delta l(s)$ in the crack plane inside the small crack front segment Δs (Fig. 2) with a crack propagation vector normal to the crack front

$$\Delta l_m(s) = l(s) \Delta a \, v_m \quad \text{with} \quad \sqrt{v_m v_m} = 1 \,, \quad \Delta l(s) = \sqrt{\Delta l_m(s) \Delta l_m(s)} = l(s) \Delta a \,, \quad (7)$$

the energy that is set free at a certain point s, is given by

$$J_m(s) \Delta l_m(s) = \left(\lim_{r \to 0} \int_C Q_{mj} n_j \mathrm{d}s \right) l(s) \Delta a \, v_m(s). \quad (8)$$

So, the total released energy for a crack, which is virtually extended by the area ΔA along the segment Δs, amounts to

$$-\Delta \Pi = \int_{\Delta s} J_m(s) \Delta l_m(s) \mathrm{d}s = \int_{\Delta s} \left(\lim_{r \to 0} \int_C Q_{mj} n_j \mathrm{d}s \right) \Delta l_m(s) \mathrm{d}s = \lim_{r \to 0} \int_{S_C} Q_{mj} n_j \Delta l_m \mathrm{d}S = \overline{J} \Delta A \quad (9)$$

whereby $\overline{J}$ represents an averaged J-value and the crack area is given by

$$\Delta A = \int_{\Delta s} \Delta l(s) \mathrm{d}s = \Delta a \int_{\Delta s} l(s) \mathrm{d}s. \tag{10}$$

In the 3D case the domain around the crack front becomes a volume V, bounded by the closed surface $\overline{S} = S + S^+ + S^- + S_{\mathrm{end}} - S_{\mathrm{C}}$ (Fig. 2).

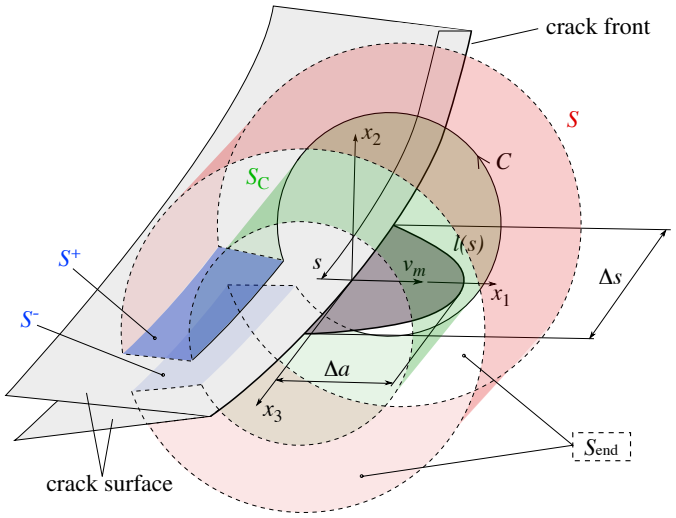

Fig. 2: Virtual displacement of the crack tip (compare Kuna (2013)).

For an efficient FEM analysis, Shih et al. (1986) developed the so-called equivalent domain integral (EDI) for homogeneous materials. In case of FGM, the released energy equation (9) can now be generalized (see Kuna (2013) for details) as follows

$$\overline{J}\Delta A = \lim_{r\to 0}\left(-\int_{\overline{S}} Q_{mj} n_j \Delta l_m \mathrm{d}S + \int_{S+S^+ +S^- +S_{\mathrm{end}}} Q_{mj} n_j \Delta l_m \mathrm{d}S\right). \tag{11}$$

Applying a smoothly varying function inside of V

$$q_m(\mathbf{x}) = \begin{cases} 0 & \text{on } S, S_{\mathrm{end}} \\ \Delta l_m & \text{on } S_{\mathrm{C}} \end{cases}, \tag{12}$$

the 3D domain J-integral at a certain crack front position s can be obtained in a way similar to the derivation of the domain integral in 2D case (compare Hein and Kuna (2014))

$$\overline{J} = J(s) = \frac{1}{\Delta A} \lim_{r\to 0} (-I_1 - I_2 + I_3) \tag{13}$$

with

$$I_1 = \int_V \left(\frac{1}{2}\epsilon^{\mathrm{m}}_{ij}\frac{\partial C_{ijkl}}{\partial x_m}\epsilon^{\mathrm{m}}_{kl} + \frac{1}{2}\epsilon^{\mathrm{m}}_{ij}\frac{\partial C_{ijkl}}{\partial T}\epsilon^{\mathrm{m}}_{kl}\frac{\partial T}{\partial x_m} - \sigma_{ij}\left(\left(\frac{\partial \alpha}{\partial x_m} + \frac{\partial \alpha}{\partial T}\frac{\partial T}{\partial x_m}\right)\Delta T(x_i) + \alpha(x_i, T(x_i))\frac{\partial \Delta T(x_i)}{\partial x_m}\right)\delta_{ij}\right) q_m \mathrm{d}V, \tag{14}$$

$$I_2 = \int_V (U\delta_{mk} - \sigma_{ik}u_{i,m})\, q_{m,k} \mathrm{d}V, \tag{15}$$

$$I_3 = \int_{S^+ + S^-} (U n_m - t_i u_{i,m})\, q_m \mathrm{d}S. \tag{16}$$

3. Thermally shocked plate with a semi-elliptical surface crack

3.1. Modeling

We consider a plate ($b = 800\,\text{mm}$, $W = 100\,\text{mm}$) with a semi-elliptical surface crack (minor axis $a = 13.85\,\text{mm}$, major axis $c = 3a$) in centered position as shown in Fig. 3.

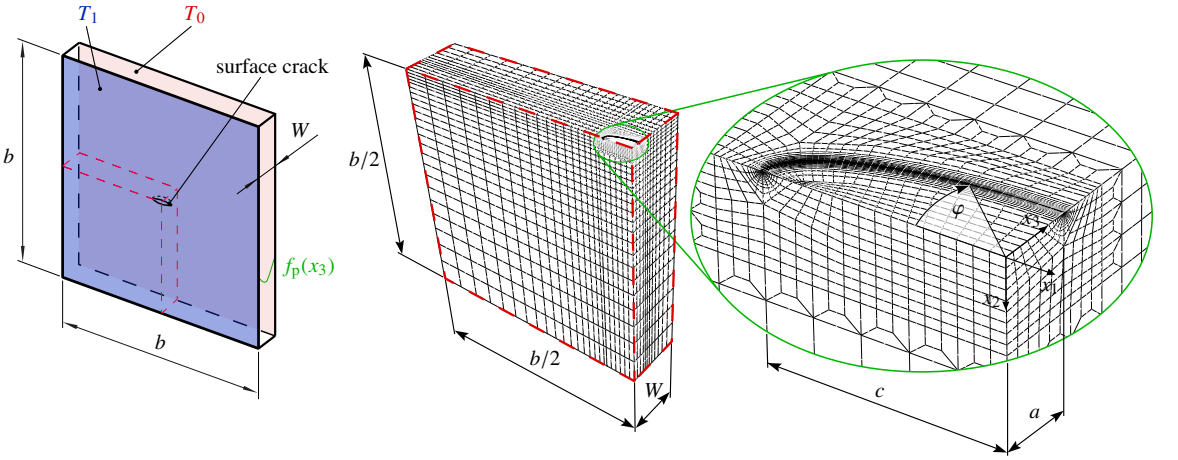

Fig. 3: Plate with 3D surface crack ; FEM-mesh: global view and detail around crack.

The plate has an initial temperature of $T_0 = 700°\text{C}$. During the thermal shock, the front surface at $x_3 = 0$ is immediately cooled down to $T(x_3 = 0) = T_1 = 300°\text{C}$, while the temperature on the back surface ($x_3 = W$) is assumed to be constant $T(x_3 = W) = T_0$ (initial temperature).
The transient heat and thermomechanical boundary value problem are solved by using the FEM-code Abaqus 6.12-3 (2012). After calculating the transient temperature fields in the plate, the thermal displacements and stresses are determined. Thereby, the outer boundaries are assumed to be stress free. Because of the double symmetry, a one quarter model (red dashed part in Fig. 3) is sufficient for consideration. Its boundary conditions are $u_1(x_1 = 0) = 0$, $u_2(x_2 = 0) = 0$ (besides of the crack face) and $u_3(x_1 = x_2 = 0, x_3 = W) = 0$.
To be able to model the material gradation and the temperature gradient within the elements, quadratic element shape functions and sufficiently small elements are used. If the elements were too big, the values of the calculated J-integrals would suffer from numerical errors and the path-independence could not be verified. More information on this crucial point is formulated by Hein et al. (2012), Hein and Kuna (2014). In order to capture the stress singularity at the crack front, the middle nodes of the crack front elements are shifted into quarter-point position. The J-integral of equation (13)-(16) is calculated as EDI by using the software J-Post 4.0 (2015) that has been developed by the Institute of Mechanics and Fluid Dynamics during the last years.

3.2. Material description

The considered FGM ceramic CaAl is manufactured and characterized by Scheithauer (2014). A material gradation has been realized by tape casting thin layers of varying porosity. Hereby, the porosity is influenced by the amount of pore forming agents ($0\,\% \le f_p \le 12\,\%$). All the material properties ($\rho, c, \lambda, E, \alpha, \nu = 0.2$) are provided as functions of temperature T for CaAl with four different concentrations of pore forming agent $f_p = \{0, 4, 8, 12\}\%$, see Fig. 4.
These functions are used to determine a description of the five varying material properties $\Phi(f_p, T)$, which is necessary to calculate $\partial\Phi/\partial x_3 = \partial\Phi/\partial f_p \cdot \partial f_p/\partial x_3$ and $\partial\Phi/\partial T$ in equation (14) for any $f_p \in [0, 12]\,\%$.

In this work, we consider three homogeneous materials $f_p = \{0, 4, 12\}\%$ (solid, dashed, dotted blue lines in the embedded small figures in Fig. 7a and 7c) and FGM described by quadratic functions $f_p(x_3) \sim x_3^2$ with $\partial f_p/\partial x_3\big|_{x_3=\tilde{x}_3} = 0$ at two different locations $\tilde{x}_3 = \{0, W\}$ (shown in the embedded small figures in Fig. 7a and 7c as red and green curves). Thereby, the two intervals $f_p = [0, 4]\%$ and $f_p = [4, 12]\%$ are investigated for grading the material.

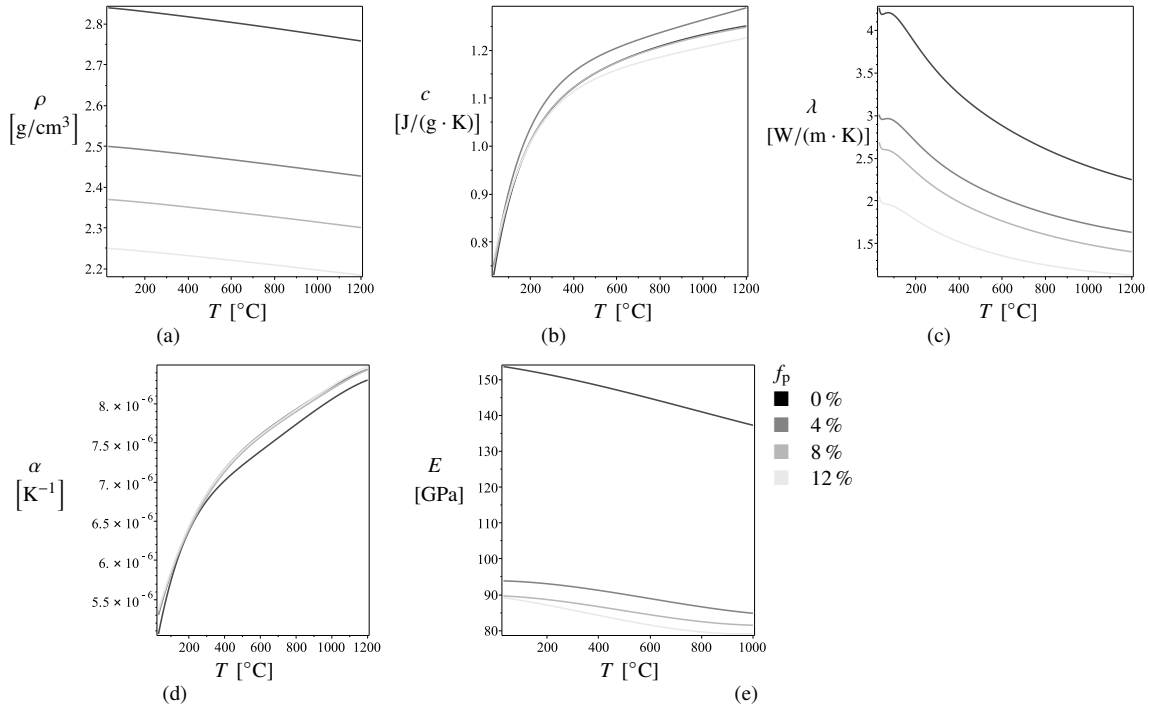

Fig. 4: Variation of material parameters with f_p and T: (a) ρ ; (b) c ; (c) λ ; (d) α ; (e) E.

Since the thermal expansion coefficients of the ceramic varieties with different pore forming agent content (Fig. 4d) are very similar, residual stresses in FGM structures do not arise during cooling down after sintering these materials together. They just may arise because of constrained shrinking, which strongly depends on the manufacturing process. Nevertheless, residual stresses are neglected in this work.

3.3. Results

The transient temperature fields across the thickness of the plate are shown in Fig. 5 for the minimal and maximal concentration of pore forming agents at selected moments of time.

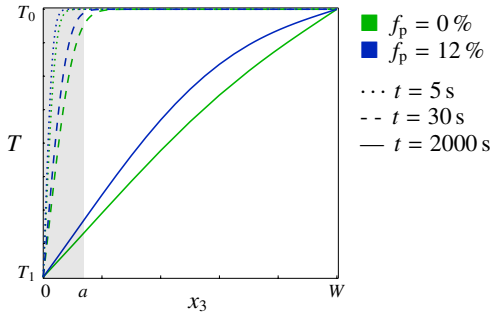

Fig. 5: Transient temperature fields across the thickness for $f_\mathrm{p} = 0\,\%$ and $f_\mathrm{p} = 12\,\%$ at $t = \{5, 30, 2000\}$ s.

The gray domain in Fig. 5 highlights that part of the plate thickness, where the semi-elliptical crack is located. Especially in the first seconds during thermal shock the temperature profiles show a steep gradient.
After determining the transient thermal stresses, the J-integral is calculated along the crack front. Here, the angle $\varphi = 0$ denotes the surface point and $\varphi = \pi/2$ the deepest apex of the ellipse, respectively. As an example, Fig. 6a shows the transient J-integral at different times for a quadratic distribution of f_p varying from 0 % to 4 %. Thereby,

J increases mostly in surface-near regions until the maximum value $\max(J) = 16.23\,\mathrm{N/mm}$ is reached at $\varphi = 0$ and $t = t^* = 20\,\mathrm{s}$. Afterwards, J decreases at the surface immediately and for $\varphi > \pi/6$ at a later time.

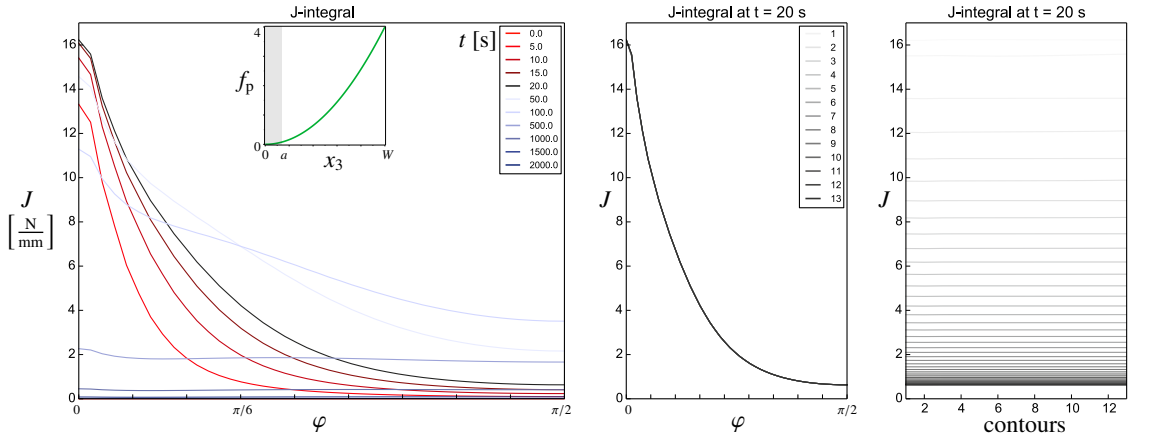

(a) J-integral along crack front at different times. (b) $J_{\max}$ of 13 contours. (c) Path-independence ($\varphi = 0 \rightarrow \blacksquare\ \varphi = \pi/2$).

Fig. 6: Quadratic FGM $f_\mathrm{p} = 0 - 4\,\%$: (a) Transient J-integral ; (b) $J_{\max}$; (c) Path-independence of J-integral at time step of $J_{\max}$.

By means of this example, the path-independence of the extended J-integral is demonstrated. This is evident from the coincident lines along crack front obtained for all contours of various radii $r \in [0.0036, 0.1852]a$ in Fig. 6b or from the horizontal lines in Fig. 6c. Hereby, $J_{\max}$ is the curve $J(\varphi, t = t^*)$ along the crack front at time t^*, at which the maximum value $\max(J)$ occurs.

The influence of material gradation expressed by concentration of pore forming agents is now studied in detail. Figures 7a and 7b show results for quadratic variations of f_p between 0 % and 4 % together with reference values obtained for homogeneous materials with these concentrations (blue lines). In an analogous manner, the concentration f_p is varied between 4 % and 12 % in figures 7c and 7d.

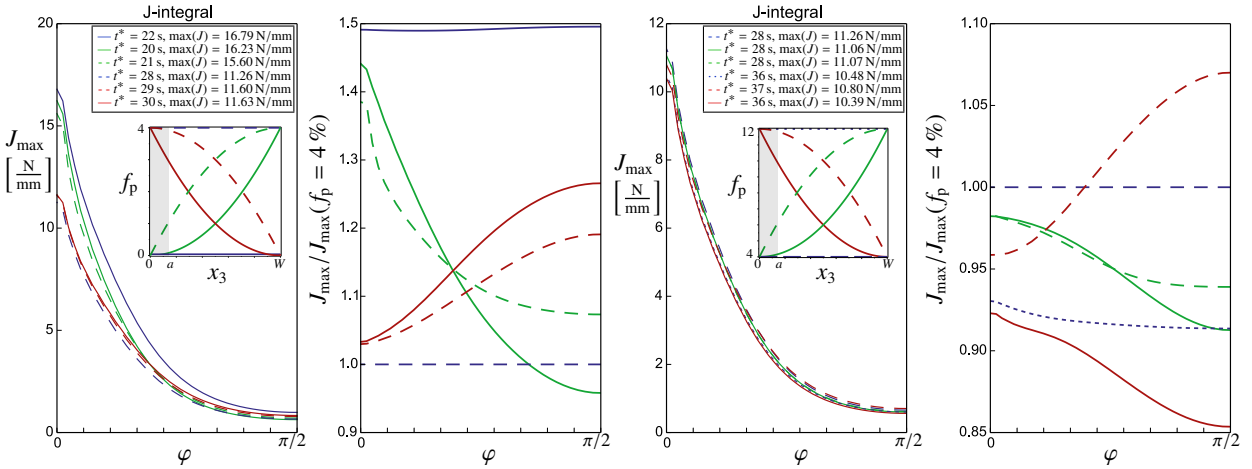

(a) $J_{\max}$ for gradations in $f_\mathrm{p} = [0, 4]\,\%$. (b) $J_{\max}/J_{\max}(f_\mathrm{p} = 4\,\%)$. (c) $J_{\max}$ for gradations in $f_\mathrm{p} = [4, 12]\,\%$. (d) $J_{\max}/J_{\max}(f_\mathrm{p} = 4\,\%)$.

Fig. 7: Comparing $J_{\max}$ of gradations: (a) and (b) $f_\mathrm{p} = [0, 4]\,\%$; (c) and (d) $f_\mathrm{p} = [4, 12]\,\%$.

The absolute values of J-integral along the crack front are depicted in figures 7a and 7c for that time t^*, where $\max(J)$ is reached. One can see from Fig. 7a that the highest and lowest curves result from the smallest and largest

homogeneous concentrations $f_p = 0\,\%$ and $f_p = 4\,\%$, respectively. All four J_{max}-curves calculated for variations of f_p lie between these extreme values. If the Young's modulus is ascending in thickness direction (red lines), then the surface-near region is less stressed and the J-values are reduced. The contrary behavior is shown by the green lines, which correspond to a descending stiffness due to higher porosity. The strong reduction of E is visible in Fig. 4e, when f_p increases from 0 % to 4 %. In order to emphasize the gradation effect, the results are presented in Fig. 7b in a manner normalized by the reference J_{max}-curve for $f_p = 4\,\%$. The substantial influence of material gradation is mainly caused by the change of Young's modulus in this case, since thermal expansion coefficient α is only little affected by f_p, see Fig. 4d. If the gradation is varied between $f_p = 4\,\%$ and $f_p = 12\,\%$, the results give another picture. The absolute J_{max}-curves show no large deviations. However, the normalized curves lie below the reference values for $f_p = 4\,\%$, i. e. the loading of the crack is relaxed (although by maximal 15 % only). This can be explained by the small difference in Young's modulus, if the amount of pore forming agent varies from $f_p = 4\,\%$ to $f_p = 12\,\%$, see Fig. 4e.

4. Conclusion

The path-independence of the thermoelastic 3D J-integral could be maintained for location and temperature dependent material parameters by adding necessary terms in the equivalent domain integral, which contain derivations with respect to coordinates and temperature. This is exemplified at a surface crack in a plate under thermal shock cooling. From the study of different material gradation functions across the plate thickness, the following conclusions can be drawn.

- Density, heat capacity and thermal conductivity affect the transient temperature field in a way that the point of time t^*, where J_{max} occurs, is retarded with increasing porosity.
- For the CaAl material under consideration, the greatest impact on J-values results from the variation of Young's modulus with respect of porosity. If the stiffness in the crack region is lower than in the depth, a favorable reduction in J_{max}-values is found and vice versa.
- However, the temperature has an opposite influence on crack loading at the cooled site.

It should be mentioned that the results represent only the crack driving side expressed by energy release rate J. This has to be contrasted with the fracture toughness of the FGM, which is also a function of porosity and temperature. The experimental determination of J_{Ic}-values for this ceramic varieties is ongoing work.

Acknowledgments

The financial support of these investigations by the German Research Foundation (DFG) under contract KU 929/16-2 within the Priority Program SPP 1418 'FIRE' is gratefully acknowledged.

References

Walters, M., Paulino, G., Dodds Jr., R., 2004. Stress-intensity factors for surface cracks in functionally graded materials under mode-I thermomechanical loading International. Journal of Solids and Structures 41, 1081–1118.

Yildirim, B., Dag, S., Erdogan, F., 2005. Three dimensional fracture analysis of FGM coatings under thermomechanical loading. International Journal of Fracture 132, 369–395.

Nami, M., Eskandari, H. Three-dimensional investigations of stress intensity factors in a thermo-mechanically loaded cracked FGM hollow cylinder. International Journal of Pressure Vessels and Piping 89, 222–229.

Moghaddam, A., Alfano, M., 2015. Determination of stress intensity factors of 3D curved non-planar cracks in FGMs subjected to thermal loading. Engineering Fracture Mechanics 146, 172–184.

Kuna, M., 2013. Finite Elements in Fracture Mechanics: Theory–Numerics–Applications, Springer Dortrecht.

Hein, J., Kuna, M., 2014. Thermoelastisches J-Integral für gradierte und temperaturabhängige Materialien. DVM-Bericht 246, 43–52.

Shih, C. F., Moran, B., Nakamura, T., 1986. Energy release rate along a three-dimensional crack front in a thermally stressed body. International Journal of Fracture 30, 79–102.

Abaqus 6.12-3, 2012. Abaqus/CAE User's Manuel. © Dassault Systèmes.

Hein, J., Storm, J., Kuna, M., 2012. Numerical thermal shock analysis of functionally graded and layered materials. International Journal of Thermal Sciences 60, 41–51.

Gloger, D., Hein, J., 2015. Dokumentation der J-Integral-Berechnungssoftware als Postprozessor für Abaqus – J-Post 4.0. Institut für Mechanik und Fluiddynamik, Freiberg.

Scheithauer, U., 2014. Private communication. Fraunhofer Institute for Ceramic Technologies and Systems (IKTS), Dresden.